IBRACON

Volume 3, Number 1 (March 2007) p. 01-14 ISSN 1809-5046

Revista IBRACON de Materiais
IBRACON Materials Journal

Mix Design and Characterization of Ultra High Performance Fiber Reinforced Cement Composites

Dosagem e Caracterização de um Compósito Cimentício de Altíssimo Desempenho Armado com Fibras

S. FORMAGINI [A]
sidiclei@mail.uniderp.br

E. M. R. FAIRBAIRN [B]
eduardo@coc.ufrj.br

R. D. TOLEDO FILHO [B]
toledo@coc.ufrj.br

Abstract

This paper presents the Compressive Packing Model (CPM) for the mix design of a self-compacting ultra high performance fiber reinforced cement composites (UHPFRCC). The concrete was produced with CPIII 40 slag cement, silica fume, silica flour, wollastonite, steel fibers and superplasticizer. The particle size of the aggregates ranged from 150 to 600μm. The input parameters for the CPM were the granulometry, the density, and the virtual compacity of the grains, together with the compaction index that corresponds to the mixing and placing protocol. New production techniques were employed, for which the addition of the several materials to the mix follows a previously defined schedule determined by the energy consumption of the mixer. The developed concrete had self-compacting characteristics. It presented compressive strength of 162 MPa at 28 days, with tensile strength of 10 MPa and modulus of rupture of 35 MPa.

Keywords: scientific mix design, compressive packing model, ultra-high performance concrete, fiber reinforced concrete, self-compacting concrete.

Resumo

Este trabalho apresenta o Modelo de Empacotamento Compressível (MEC) para a dosagem de um compósito cimentício de altíssimo desempenho armado com fibras (CONADAF). O concreto foi produzido com cimento CPIII 40, sílica ativa, quartzo moído, areia natural, dispersante, microfibras de wollastonita e fibras de aço. A dimensão das partículas dos agregados variou entre 150 e 600μm. Propriedades dos materiais, como distribuição granulométrica dos grãos, massa específica e compacidade virtual, assim como o índice de compactação que corresponde ao protocolo de mistura e colocação do material foram utilizados como parâmetros de entrada do MEC. Novas técnicas de produção foram introduzidas, com adição dos líquidos à mistura em função da demanda de energia requerida pelo misturador. O concreto demonstrou ser auto-adensável e apresentou valores de resistência à compressão aos 28 dias de 162 MPa, com resistência à tração direta de 10 MPa e módulo de ruptura de 35 MPa.

Palavras-chave: dosagem científica, modelo de empacotamento compressível, concreto de altíssimo desempenho, concreto armado com fibras, concreto auto-adensável.

[a] *Adjoint Professor, Civil Engineering Course, UNIDERP, sidiclei@mail.uniderp.br, Cx. 2153, Campo Grande, MS, Brazil*
[b] *Associate Professor, Civil Engineering Department COPPE/UFRJ, eduardo@coc.ufrj.br, toledo@coc.ufrj.br, Cx. 68506, Rio de Janeiro, RJ, Brazil*

1 Introduction

Recent developments in the mix design technology combined with the use of ultra-fine materials have allowed the development of ultra-high performance fiber reinforced cement composites (UHPFRCC) which have excellent properties, both in the fresh state (workability and self-compacting capability) and in the hardened state (extremely high compressive strengths and high tension ductility), in addition to high durability (thick microstructure, low porosity, high chemical resistance) [1]. The UHPFRCC development has been possible thanks to the application of scientific mix design methods leading to packing optimization, use of additives affecting rheology and to the constituent chemical reactivity [2]. The use of reinforcing steel fibers increases the material ductility, reducing trend to development of fragile ruptures, which trend can be seen in more homogeneous materials such as high and very high performance concretes ([3], [4]).

This paper presents an UHPFRCC mix design methodology, based upon the maximum dry granular mix packing concept, using the compressive packing model (CPM), developed by DE LARRARD and collaborators ([5],[6],[7]). Mix design through CPM, in addition to taking into account traditional parameters such as slump test and compressive strength, allows for more complete material characterization by using a higher number of parameters defining the physical-chemical phenomena such as: cinematic viscosity and shear stress, considering the fresh composite as a non-Newtonian fluid, modulus of elasticity, heat of hydration and autogenous shrinkage for the hardened concrete.

The mix is processed by means of innovative techniques, entirely different from the traditional ones, for being a composite produced with high cement amounts, high superplasticizer contents, aggregates with 600 μm maximum dimension and 0.19 water-to-cement ratio (w/c) [8].

2 The Compressive Packing Model (CPM)

2.1 Initial conceptualization

One of the most important concepts for the CPM development is the virtual packing compacity (β) of a mono-dispersed granular mix (mix of grains considered as having constant diameter), defined as the maximum possible compacity through stacking of grains one by one and/or with the use of a high amount of energy (but without breaking the grains) [5]. A theoretical, yet clarifying example, is the case of equal cubes which would have a virtual packing compacity β=1 if piled one by one (Figure 1a). Another example is the stacking of equal-size spheres, for which the virtual compacity is β=0.74, which corresponds to the FCC (Face Centered Cubic) crystalline structure that can be seen in nature, e.g., in copper and gold atoms (Figure 1b).

The virtual compacity (β) of a given grain class is an intrinsic property of this class and is not dependent on the actual packing protocol to which it was submitted, since β is defined according to an ideal (virtual) packing protocol. The virtual packing concept described above can be extended to a mix of grains pertaining to several different granulometric classes. In this case, the virtual mix compacity is denominated by the Greek letter γ.

Another important concept for preparation of CPM is the one of the dominant grain class. Thus, if it is set up that grain class diameters are ordered in the sequence $d_1 > ... > d_i > ... > d_n$, and if there is no segregation, we say that the grain class i is dominant if it assures solid continuity of the grain body, as shown in Figure 2. In this example of binary mix ($d_1 > d_2$), the solid continuity is assured by grains class 1, and lower size class grains just occupy part of the voids produced by packing of the largest size class grains.

Figure 1 – Packing arrays

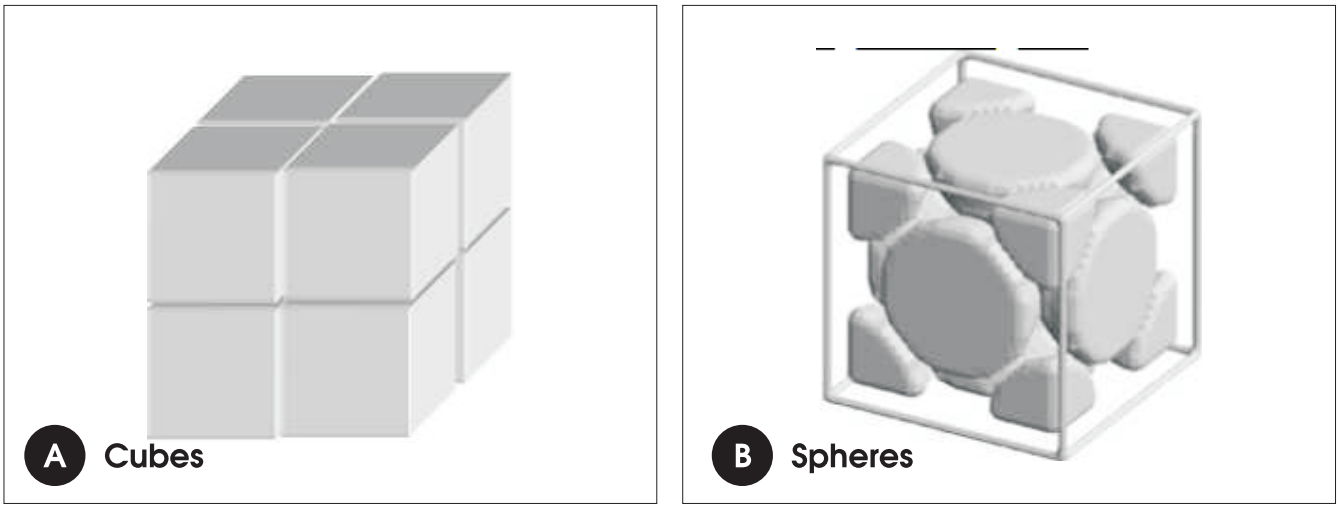

Figure 2 – Dominant class concept (6)

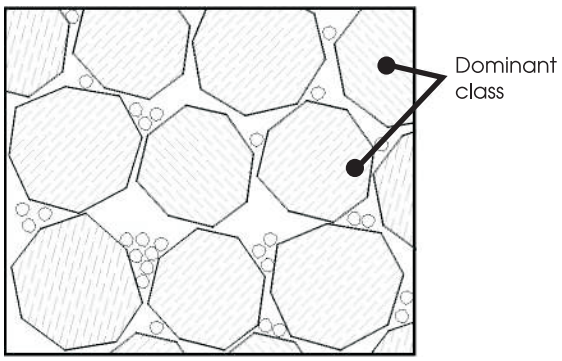

The CPM can be understood as a model built in two modules: In the first module, algebra is established, which deduces the virtual packing ratios.
In the second module, the ratios (mostly physical and experimental) connecting the virtual properties (mainly heuristic, which characterize the material capability to pack) to the actual properties of granular mix submitted to a packing procedure, are established. For example, if a vessel is considered with a high number of spherical particles, they would never reach 0.74 compaction.
Then, the CPM relates the virtual packing to the real packing through an intrinsic parameter to the real packing procedure adopted, called compaction index. Any such index is a scalar, called K, and correlates the virtual compacity (γ) with the real compacity (ϕ). This scalar depends on the pouring and compacting protocol required for the mix design. When the value of K tends to infinite, the compaction ϕ tends to virtual compacity γ.
The K index value is deduced from binary mixes, according to the pouring protocol adopted. Table 1 [6] presents values for the K index for several types of protocols, used for characterizing materials.

Table 1 – Values of compaction index for several conditions of pouring and compacting

	Packing protocol	K
Dry	Simple pouring	4.1
	Pounding	4.5
	Vibration	4.75
	Vibration + compression 10kPa	9
wet	Water demand	6.7
virtual	(one by one, manually (γ))	∞

2.2 Formulation

The general equation representing the virtual compacity ($\gamma^{(m,i)}$) of a granular mix compounded by m materials divided in n classes, when class i is dominant, is given by [7]:

$$\gamma^{(m,i)} = \frac{\beta_{mi}}{1-\sum_{K=1}^{M}[\delta_1+\delta_2]} \qquad (1)$$

Being:

$$\delta_1 = \sum_{j=1}^{i}\left[1-\beta_{mi}+b_{ij}\beta_{mi}\left(1-\frac{1}{\beta_{kj}}\right)\right]p_k y_{kj}$$

and

$$\delta_2 = \sum_{j=i+1}^{N}\left[1-a_{ij}\frac{\beta_{mi}}{\beta_{kj}}\right]p_k y_{kj}$$

Where:
p_k is the volumetric fraction of material m;
y_{mi} is the volumetric fraction of class i of material m;
β_{mi} is the virtual compacity of class i of material m.

Coefficients a_{ij} and b_{ij} represent, respectively, the effects of loosening and wall exercised by grains when packed.
The general equation, for a mix of m materials divided into n classes, which relates the virtual compacity to the real compacity through the compaction index (K), is given by [7]:

$$K = \sum_{i=1}^{M}\frac{\sum_{m=1}^{M}\frac{p_m y_{mi}}{\beta_{mi}}}{\frac{1}{\phi}-\frac{1}{\gamma^{(i)}}} \qquad (2)$$

As can be seen, the equation (2) is implied in φ and demands, from a ternary mix, a numeric procedure for its resolution. However, the search space is limited and robust resolution procedures may be used.
Equation (2), if particularized for a mono-dispersed grain class allows for virtual compacity (β) from the real compacity (φ) to be determined through a trial test which corresponds to a given packing protocol, the compaction index K of which is known. Thus, the virtual compacity can be determined by the formula:

$$\beta = \phi\left(\frac{1}{K}+1\right) \qquad (3)$$

The CPM operationalization, in order for the compacity calculation of granular mix to be able to be performed, demands the trial determination of the several properties of each material, such as granulometry, density and the experimental compacity, in addition to knowledge of the value of K index for the packing protocol used.
With such values and equations (1) to (3), it is possible, through an optimization procedure, to determine the composition of the several materials which supplies the highest compacity for materials used.
In addition to determination of this optimum mix, which corresponds to the maximum compacity, the CPM, through specific models, can also be used for forecasting some of the composite properties both in the fresh and in the hardened state. Any such models will be presented next.

2.3 Determination of fresh composite properties

Within the CPM framework, the fluid model used for the composite is the Bingham one, for which till a limit shearing stress τ_0, is reached, the material behaves as a solid, and then there is a linear relation between shearing stress τ and angular strain rate $\dot{\gamma}$. This model is represented by the following equation:

$$\tau = \tau_0 + \mu \dot{\gamma} \quad (4)$$

where μ is the plastic viscosity. Figure 3 indicates, schematically, that flow stress τ_0 originates from the contact between grains and that cinematic viscosity is related with the viscous dissipation of the liquid.
Thus, in model proposed by CPM, the plastic viscosity (μ) is associated with the normalized solid concentration (ϕ_t / ϕ_t^*), where ϕ_t is the volume of solids of class i

Figure 3 – Fresh state composite behavior (6)

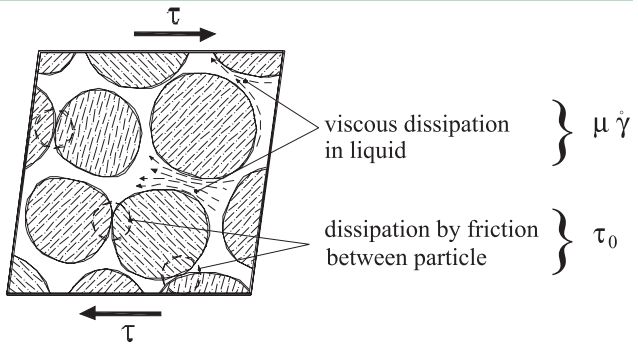

and ϕ_t^* is the maximum volume that can be occupied by class i in presence of other classes:

$$\mu = \exp\left[26.75\left(\frac{\phi}{\phi^*} - 0.7448\right)\right] \quad (5)$$

For the limit shearing stress τ_0, the CPM proposes the following expression:

$$\tau_0 = \exp\left(2.537 + \sum_{i=1}^{N} a_i \frac{\phi_i / \phi_i^*}{1 - \phi_i / \phi_i^*}\right) \quad (6)$$

where: the sum i= 1,N refers to the several grain classes, and index 1 refers to the cement and the subsequent indices to the aggregates; coefficient a_1, which depends on the superplasticizer content in the mix being given by:

$$a_1 = 0.224 + 0.910\left(1 - S_p / S_p^*\right) \quad (7)$$

with S_p and S*p, being, respectively, the superplasticizer mix design and its saturation point; coefficients a_i, with i ≥ 2, are related with the grains size and determined by the following relation:

$$a_i = 0.736 - 0.216 \log(d_i) \quad (8)$$

where d_i (mm) is the mean diameter of aggregates in granular class i.

2.4 Determination of hardened composite properties

The cement matrix compressive strength, in terms of age t, is determined by the expression [6]:

$$f_{cm}(t) = 13.4\, Rc_{28}\, MEP^{-0.13} \times \times \left[d(t) + \left(\frac{\upsilon_c}{\upsilon_c + \upsilon_w + \upsilon_{ar}}\right)^{2,85}\right] \quad (9)$$

where: Rc_{28} is the cement compressive strength in 28 days

(MPa); υ_c, υ_w and υ_{ar} represent, respectively, the volumes of cement, water and air in a unitary volume of composite; d(t) is a dimensionless kinetic parameter, which represents the cement contribution in the composite strength at an age t, determined by:

$$d(t) = 0.0522\left(\frac{Rc_t}{Rc_{28}} - 1\right) \quad (10)$$

Being: Rc_t the cement compressive strength at age t; MEP the maximum paste thickness (average distance between aggregates immersed in matrix as shown in Figure 4), determined by the expression:

$$MEP = D\left[\sqrt[3]{\frac{g^*}{g}} - 1\right] \quad (11)$$

where: D is the aggregate dimension relating to 90% percentage passing a previously defined screen; g is the real volume of aggregates in a unit volume of composite; and g* is the real compacity of aggregates determined as index K = 9.
The modulus of elasticity of cement matrix E_m (GPa), in terms of age t, is given by [6]:

$$E_m(t) = 226 f_{cm}(t) \quad (12)$$

The cement matrix tensile strength, corresponding to direct tensile test is obtained by [6]:

$$f_t(t) = 0.468 f_{cm}(t)^{0.57} \quad (13)$$

2.5 Computer simulator

Based on the concepts presented in items 2.1 through 2.4 and represented schematically by equations (1) through (13), a mix computer simulator has been developed which allows optimization of compacity and calculation of material properties in both the fresh and hardened states. The simulator, referred to as MECFOR, is described in details in reference [1].

Figure 4 – Maximum paste thickness in a dry granular mix (6)

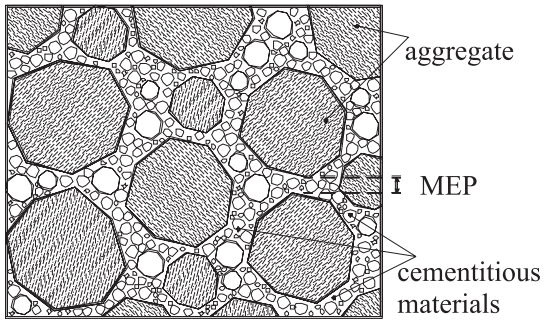

3 Experimental characterization of UHPFRCC components

3.1 Materials employed

Cement materials used were slag cement CPIII 40 (CP) and silica fume (SF). Three types of aggregates, namely: silica flour (Q) with 18 μm average size; and two mono-sized classes of natural sand (screened), with grain size ranging from 150 μm to 300 μm (C1) and from 425 μm to 600 μm (C2), respectively. A superplasticizer (SP) has been used based on polycarboxylates with 32.5% solids. 2% volume of steel fibers (SF) (12 mm long and 0.18 mm in diameter) and 2.6% wollastonite (W) micro-fibers (with transverse dimension ranging from 5 μm to 100 μm and longitudinal dimension ranging from 50 μm to 2 mm), were used as reinforcement with no building up of balls,

Figure 5 – Granulometry

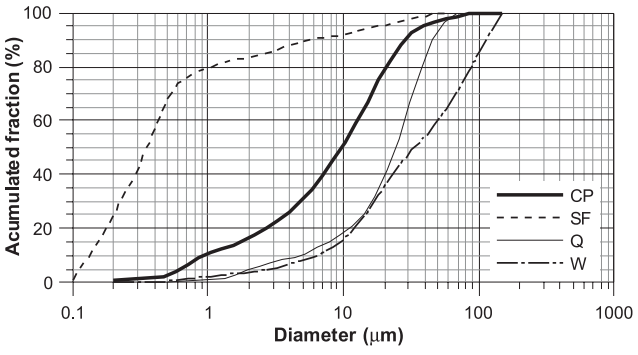

Table 2 – Density of materials (g/cm³)

CP	SF	Q	C1	C2	W	SF
2.99	2.22	2.65	2.67	2.67	2.9	7.9

Table 3 – Chemical composition

Compound	CP	SF	Q	W
Fe_2O_3	2.62	0.70	0.10	0.40
CaO	52.14	1.10	0.30	47.5
K_2O	0.51	0.44	—	—
Al_2O_3	7.50	0.10	0.20	0.20
SiO_2	24.94	91.00	98.80	51.00
MgO	5.34	1.50	0.20	0.10
SO_3	2.57	—	—	—
CO_2	1.51	—	—	—
Na_2O	0.09	0.39	—	—
Losses	2.63	—	0.40	0.68

Table 4 – Disperser characteristics

Type	density	pH	% solids
Polycarboxylates	1.04-1.11	6-7	32.0-33.1

satisfying self-compacting criteria set up for the composite. The a / c ratio was 0.19.

3.2 Experimental characterization

3.2.1 Granulometry

Granulometry of CP, Q and of W was determined by the laser granulometry test. For the SA, sedigraphy technique has been used. Material granulometry is shown in Figure 5.

3.2.2 Density

The density values for CP, SF and Q were determined by means of Le Chatelier flask according to procedures set up by NBR NM 23 [9]. Density of each sand class has been determined by means of Chapman flask according to NBR 9776 [10]. Density of W was supplied by manufacturer. Values so obtained are presented in Table 2.

3.2.3 Chemical composition

Chemical compositions of cement materials, of Q and of W, supplied by their respective manufacturers are presented in Table 3.

3.2.4 Superplasticizer

Characteristics of superplasticizer used have been determined on a trial basis and are presented in Table 4. Its compatibility and saturation point with cement materials have been determined by means of the paste fluidity test, using the Marsh funnel with 5mm opening [11]. Results are shown in Figure 6.

3.2.5 Compacity

The experimental compacity of fine materials (d <100 µm) was determined by the water demand test (K index =6.7, Table 1) [6]. This test, conducted in a bench mixer (Figure 7), consists of adding water to a standard sample of dry dusts till they present a homogeneous paste aspect with fluidity properties, indicating qualitatively the filling of all voids with water.
The experimental compacity of materials the size of which is above 100 µm is determined by the vibration protocol plus 10

Figure 6 – Disperser saturation point with CP, SF and Q

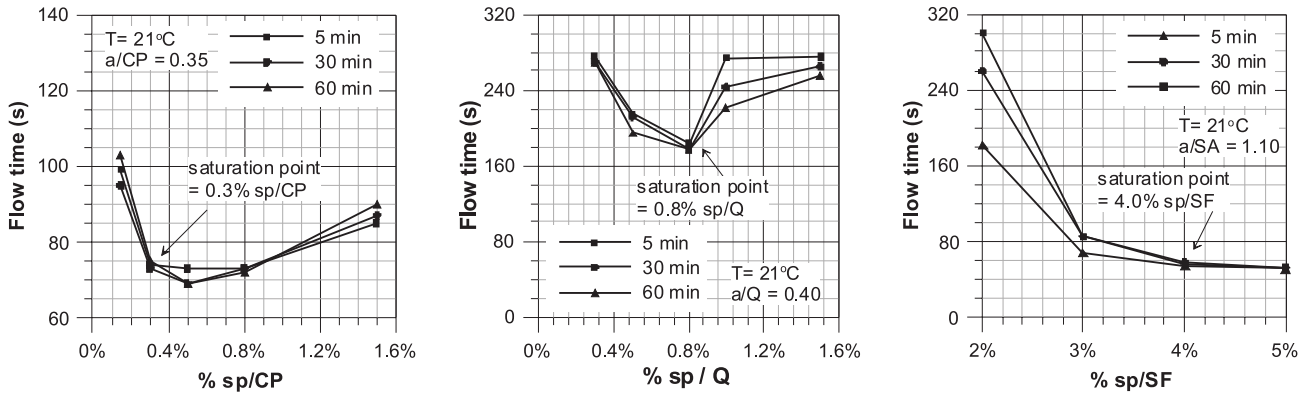

Figure 7 – Water demand test

Figure 8 – Vibration test plus 10 kPa (K=9) pressure

kPa compression (K=9 compaction index, Table 1). The test, conducted in a hollow cylinder equipped with a piston and coupled to a vibratory table (Figure 8), consists of applying pressure and vibration to a pre-defined material mass generating maximum real packing of mix [12]. Height of piston is then measured being related with the dry granular mix compacity.
The compacity experimental values, obtained according to procedures described above, are shown in Table 5.

Table 5 – Experimental compacity

Materials	K	% sp	ϕ
CP	6.7	0.3	0.636
SF	6.7	4.0	0.438
Q	6.7	0.8	0.680
W	6.7	0.8	0.438
C1	9	—	0.593
C2	9	—	0.594

4 Mix design and production

4.1 Concrete mix design determination

In order to assure ultra-high performance properties to the UHPFRCC in the fresh and hardened states, the following principles have been considered for preparation of mix design [2]:

- Utilization of aggregates with reduced sizes in order to assure macroscopic homogeneity of granular mix;
- Optimization of granular mix compacity using tools presented in 2;
- Increased ductility through addition of multi-scale fiber reinforcement, namely, SF and W;

The UHPFRCC mix design has been determined by the MECFOR program [1], with volumetric fraction of materials optimized in terms of the maximum compacity allowed by the constituents of the granular mix for a compressive strength above 150 MPa. In preparing the mix design, specifications presented in Table 6 were adopted [6]. The disperser mix design corresponded to the cement mix saturation point. Volumetric fractions of wollastonite and steel fibers have been set at respectively 2.63% and 2.0%, with the mix properties being maintained, in the fresh state, adequate to pouring without any balls being built up.
The optimized concrete mix design for UHPFRCC, as well as some properties in the fresh and hardened states, for which it was adopted, is presented in Table 7.

Table 6 – UHPFRCC specification

Criterion	Value
Spreading	≥ 600 mm
Plastic viscosity (μ)	≤ 200 Pa.s
Volume of aggregates	≥ 30%
Compressive strength	maximum

4.2 Mix criteria

The kinetics of transformation of a cement mix (dry materials and water) in a homogeneous paste is influenced by three factors: mixer type, strength and rate; ambient temperature and temperature of materials used; and addition time of liquids and fibers to the mix.
The mixer should be planetary type, as it supplies a higher degree of homogeneity, thus facilitating dispersion of grains during the mix, since it is processed with very few water and materials with sizes below 600 μm. Besides, the transformation kinetics is highly influenced by the appearance of forces at the surfaces of fine particles when contacting water.
The materials, before being placed in the mixer, should preferably remain at a temperature below 21°C so that, during mixing, the temperature is not increased excessively, which would favor the surface desiccation phenomena.
The order of addition of materials to the mixer is also very important. Liquids and steel fibers should be added according to sequence presented in sub-item 4.3.

Table 7 – Optimized concrete mix design for UHPFRCC

Materials	Fraction vol.	Consumption (kg/m³)
CP	0.3381	1011
SF	0.0261	58
Q	0.0301	79
C1	0.0225	60
C2	0.3082	823
W	0.0263	76
SF	0.0200	158
Superplasticizer	0.0450	50
Water	0.1626	162
Trapped air		3.75
Water/cement ratio	0.19	
Water ratio/(C+SA)	0.17	
Compacity (ϕ)	0.7555	
Compacity (ϕ^*)	0.7737	
Aggregate volume (g)	0.3327	
Aggregate volume (g*)	0.6069	
MEP (mm)	0.1292	
Plastic viscosity (μ) (Pa.s)	200	
Shearing stress (τ_0) (Pa)	434 Pa	
Pouring and compaction (K*)	7.475	
Compressive strength (28 days) (MPa)	154.9	
Direct tensile strength (28 days) (MPa)	8.29	
Modulus of elasticity E_m (28 days) (GPa)	35.0	

The mix operation should be conducted in such a way that optimum constituent dispersion occurs, without excess elevation of the mix temperature or build up of steel fiber balls, compromising their properties in the fresh and hardened state.

4.3 Production

In order to produce UHPFRCC, different techniques are adopted from those used in production of conventional concretes, requiring special care during mixing.
The moment of addition of liquids and steel fibers to the mix has been monitored and controlled through energy consumption required by the planetary mixer (Figure 9a) to process the mix. This procedure was implemented at COPPE/UFRJ (university of Rio de Janeiro) by BRANDÃO [8], aiming at standardizing the exact time of addition of liquids and steel fibers, as well as the moment of its completion. Power required by mixer has been measured by a digital wattmeter, connected to the mixer power supply and connected to a computer (Figure 9b), the signals

Figure 9 – Mixer power control

of which are processed by a data acquisition system and presented graphically in real time.
Figure 10 indicates the moments of addition of liquids and steel fibers to the mix.
The dry materials and the wollastonite micro-fibers, previously weighted, were firstly added to the planetary mixer (Figure 11a). Then, the mixer was turned on and the mix was allowed to homogenize for 1 minute, carefully so as to keep dust from being spilled off the mixer (Figure 11b). In the sequence, the liquids and the steel fibers were added in the following order: (i) half of the superplasticizer diluted in half of the mixing water; (ii) the other half of the mixing water; (iii) the other half of the superplasticizer; (iv) steel fibers.
After the sequence (i), the first particle agglomerates were formed (Figure 11b) and, when passing through this stage, the mix presented aspect of "wet soil" (Figure 11c). The second half of water was then introduced (Figure 11d). At this time, particle agglomerates with larger sizes could be clearly seen. As those particle agglomerates increased size, they were broken by the rotating mixer blade. The water, which was trapped inside, started to be released to the mix, causing significant increase in the mixer demand for energy. When the peak demand for energy was

Figure 10 – Mixing phases related with mixer power consumption

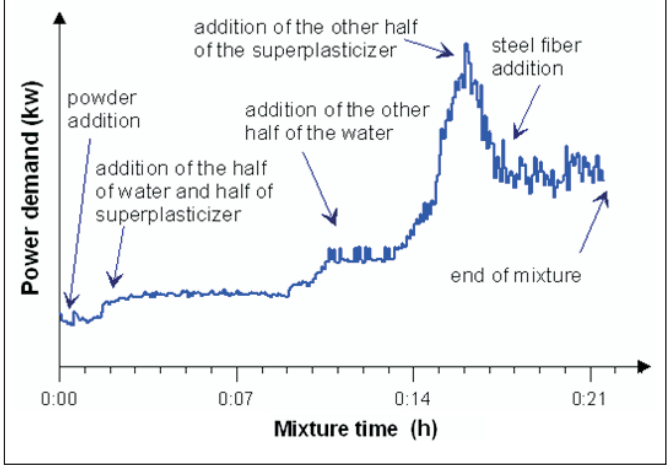

well defined, the second half of disperser was introduced (Figure 11e). The mix then presented an aspect of rigid paste reaching the reversion point (peak demand for energy, Figure 10). After the reversion point (Figure 11f), the mix became more and more fluid and, upon forming a horizontal plateau (Figure 10), the steel fibers were added continuously to the moving mix (Figure 11g). Care should be taken so as to avoid extending the mixing beyond this point in order to keep excess elevation of the paste temperature from occurring (or local evaporation) and to avoid the risk of accelerating the surface drying or desiccation of the composite.

Figure 11 – UHPFRCC mixing steps

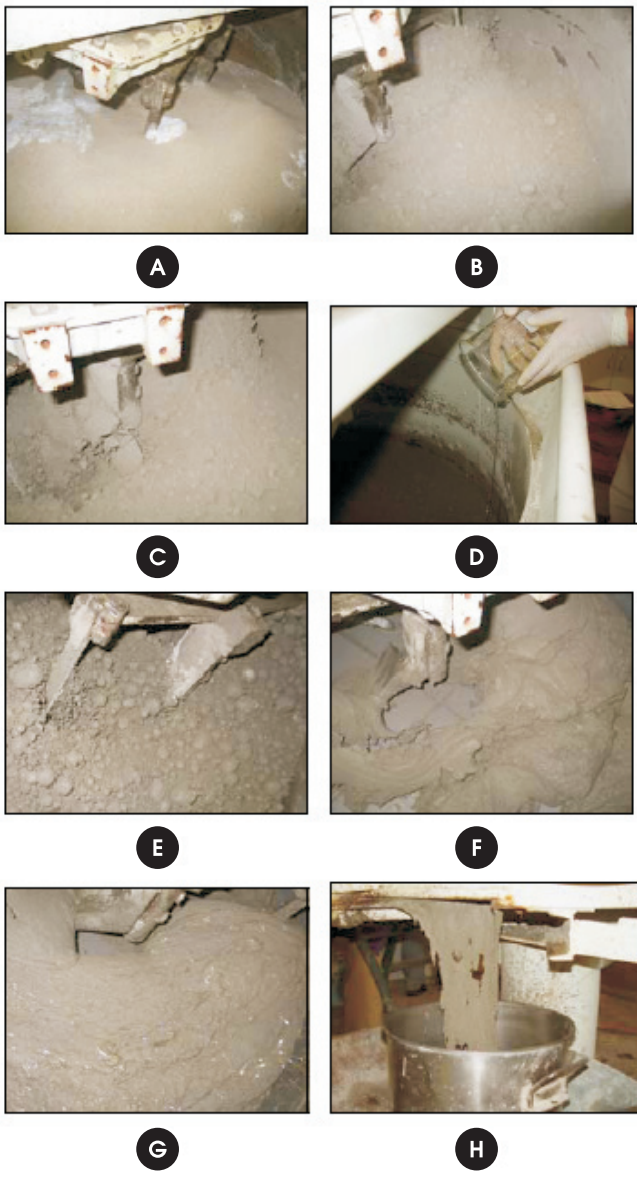

Figure 12 – Self-compaction test

The mixer having been turned off, the composite was placed in vessels (Figure 11h) to be transported to the different equipment for broad characterization in the fresh state and to be poured in moulds for characterization in the hardened state.

5 UHPFRCC characterization tests

The following sub-items present a brief description of methodologies of the several tests conducted for mechanical characterization of UHPFRCC.

5.1 Fresh state

The properties in the fresh state have been evaluated from the self-compacting tests using an L-shaped box and spreading through the inverted slump test.

5.1.1 Self-compaction

Self-compaction check was conducted by the flow test, using an L-shaped rectangular section box (Figure 12), with horizontal and vertical section separated by a detachable cover. The test consists of measuring the mean flow time of the composite through the lower opening and checking the box bottom for leveling.

5.1.2 Slump

The mean composite spreading diameter is determined through the Marsh cone slump test, the cone being po-

Figure 13 – Slump test

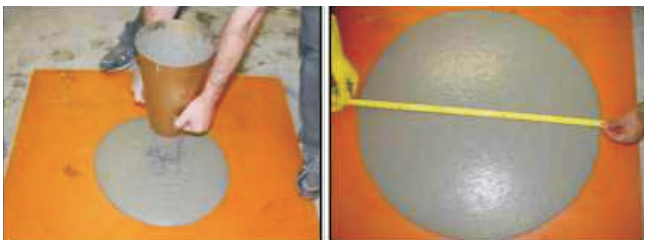

sitioned inverted over a metallic base, as illustrated in Figure 13.

5.2 Hardened state

In the hardened state, the autogenous shrinkage, modulus of elasticity, compressive strength, direct tensile strength and bending strength were evaluated.

5.2.1 Autogenous shrinkage

The autogenous shrinkage was checked through the ten prismatic-element test, the dimensions being 71 x 73 x 276 mm. The tests were conducted according to methodology proposed by TAZAWA and EI-ICHI [13]. In order to reduce friction between the composite and the mould walls, a 2 mm thick teflon film was added before molding. Two J-type iron-constantan thermocouples were added to the elements to control temperature variation since the test beginning. Temperature was measured continuously by means of a data acquisition system during the first 120 hours.
Two pins were provided at each end of the specimen, which were embedded after pouring of concrete, being used as a base for longitudinal dimension measurements. The moulds, upon being filled, were isolated externally with plastic film and adhesive tape in order to avoid humidity loss to the environment (Figure 14a). The specimens remained in an acclimated room at 52 ± 4% relative humidity and 19.5 ± 1°C temperature up to the test completion.

Figure 14 – Autogenous shrinkage measurement

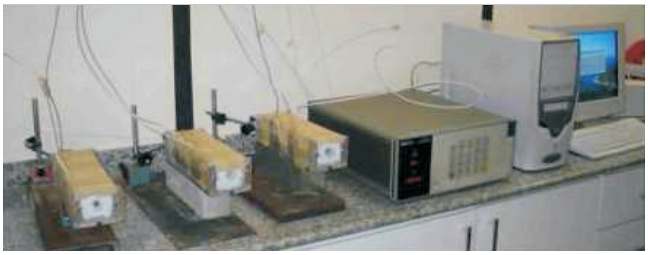

A Monitoring of internal temperature variation

B Inside the mould

C Outside the mould

Figure 15 – Tests conducted for mechanical characterization of UHPFRCC

A Compression

B Plate bending

C Prism bending

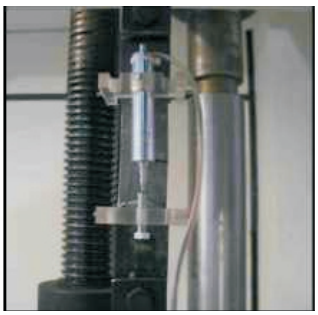

D Direct tension

Two micrometer sensors (Figure 14b) were used for performing longitudinal dimension measurements, while the specimen remained inside the mould (first 5 days). The first reading was performed 16 hours after completion of molding. At 5 days of age, the test specimens were removed from the moulds and sealed with aluminum tape, preventing water loss by evaporation into the environment. As of this date, the autogenous shrinkage was measured with the test specimen embedded in a vertical gantry, as shown in Figure 14c. Deformation was read in 60-minute interval during the first 120 hours and then at every 12 hours, at more advanced ages.

5.2.2 Strengths and modulus of elasticity

Properties evaluated were compressive strength and modulus of elasticity (Figure 7a) through cylindrical test specimen test (50 x 100 mm); tensile strength (Figure 7b-c) through the four points bending test in plates (100 x 20 x 400 mm) and prisms (100 x 100 x 400 mm); and tensile strength (Figure 7d) through the direct tension test in plates (12 x 50 x 200 mm).
The mechanical tests were conducted in a servo-controlled Shimadzu machine, with 1000 kN load capacity. The uniaxial compressive strength test was conducted with axial strain control at a rate of 0.005 mm/min. The axial strain of the test specimen was read from the average supplied by two electric displacement transducers (LVDT), coupled

Figure 16 – Mean autogenous shrinkage curve

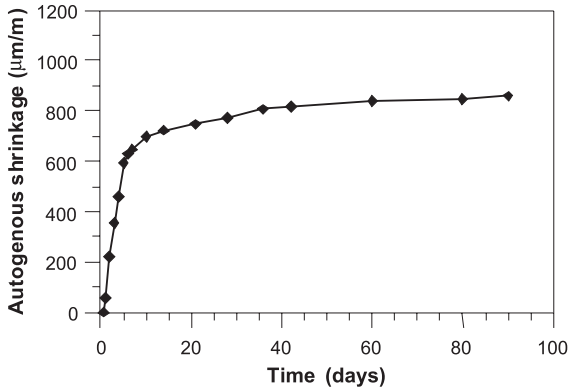

by metallic rings positioned at the central region of the test specimen. The four points bending test was conducted with displacement control of the stroke at a rate of 0.1 mm/min. Deflection in mid span was measured by a LVDT fastened to a metallic support. The direct tension test was also conducted with stroke displacement control at a rate of 0.1 mm/min. Elongation was measured by means of two LVDTs positioned at opposite sides of the test specimen.

6 Presentation and analysis of experimental results

6.1 Fresh state properties

The test result using the L-shaped box indicated that the composite is self-compacting. The mean flow time through the lower opening for self-leveling at the box bottom was 30 seconds. After the test, the entire composite became leveled at the lower part of the box.

The mean composite spreading diameter in the Marsh slump test was 73 cm.

Table 8 – Compressive strength and Modulus of Elasticity

Age (days)	Number of cps	fcm (MPa)	DP (MPa)	Em (GPa)	DP (GPa)
3	5	74.3	1.8	35.6	2.2
7	4	111.0	3.8	43.0	1.4
28	4	162.1	3.1	47.7	1.4
180	3	181.3	5.2	51.6	0.9
365	3	190.0	3.0	53.7	0.3

6.2 Autogenous shrinkage

The autogenous shrinkage test results are shown in Figure 16, where one can see the rapidity of the phenomena at the first ages. Results presented correspond to the average value, which has 10.5% coefficient of variation. The mass loss of elements measured during the test was lower than 0.08%, indicating that sealing of the test specimens was effective.

6.3 Compressive strength and modulus of elasticity

Typical tension-strain behavior curves under compression for different ages (3, 7, 28, 180 and 365 days) under wet cure conditions are shown in Figure 17. Table 8 presents the average of experimental results of compressive strength and modulus of elasticity. By analyzing the tension-strain curves, one can see higher linearity at the first ages (3 and 7 days) than at more advanced ages (28 to 365 days).

Figure 17 – Typical tension-deformation behavior curves under uniaxial compression

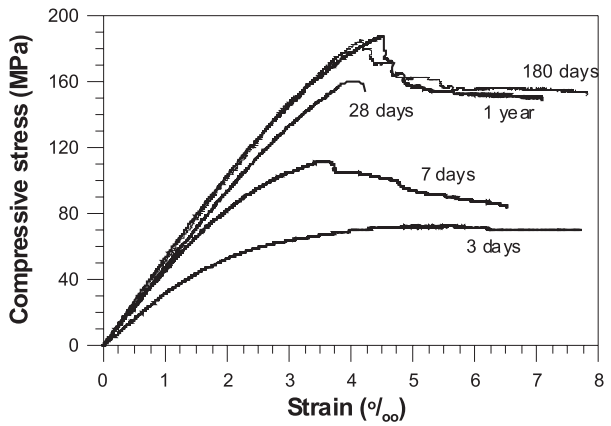

Figure 18 – Theoretical versusexperimental comparison of compressive strength

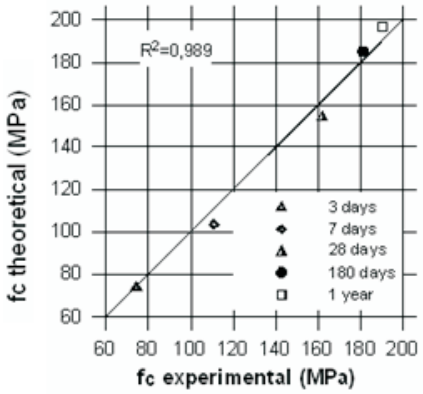

Figure 19 – Typical mid-span equivalent spring tension curves in flexion versus deflection

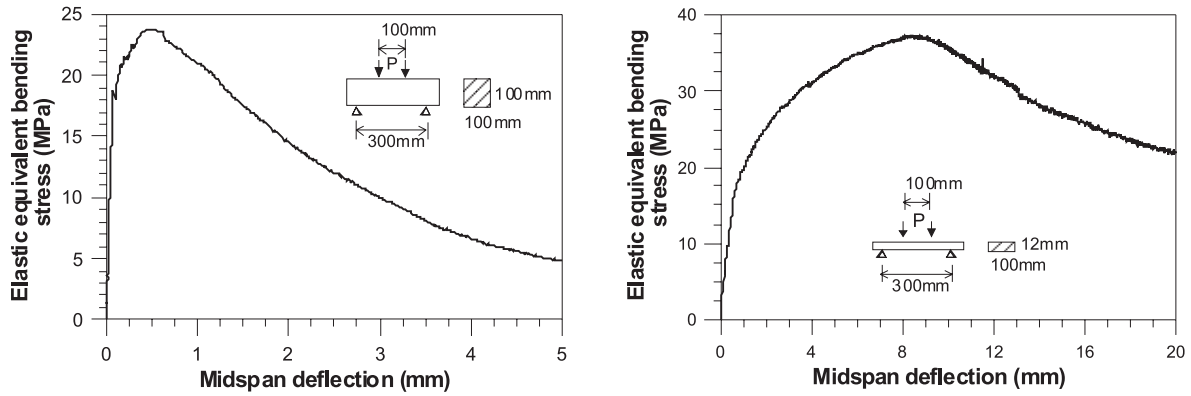

Figure 18 presents a comparison between results supplied by CPM and experimental methods of compressive strength of composite for ages 3, 7, 28, 180 and 365 days. For the produced composite, the correlation coefficient relating to compressive strength presented the value of R^2=0.989 indicating good accuracy of the model. As for the modulus of elasticity, the model presented good correlation.

6.4 Four-point bending test

Typical equivalent tensile stress curves ($\sigma = 6M/bd^2$) in bending versus deflection in mid span obtained at 28 days for the prisms and for the plates are shown in Figure 19.

Both figures highlight the ductile nature of UHPFRCC. For prisms, a mean first crack stress was obtained of 18.2 MPa (with 4.3% CV) at deflection of approximately 0.08 mm while the maximum post-crack stress of 23.0 MPa (with 3.0% CV) was obtained at a deflection of approximately 0.4 mm. For the plates, a mean first crack tension was obtained of 17.3 MPa (with 3.3% CV) at a deflection of approximately 0.6 mm while the maximum post-crack stress of 35 MPa (with 9.7% CV) corresponded to a deflection of approximately 7.9 mm, due to the multiple crack at the region of maximum bending moment (Figure 20). In both cases, after the peak load, localization and prolongation of a main crack was observed, and the occurrence of a strain-softening behavior of the load-deflection curve could be verified. A significant scale effect can be observed between results obtained for the prism and for the plate, both concerning the ultimate load, and ductility of test specimens tested. Any such effect matches trials previously conducted and reported in the technical literature [14].

Figure 20 – Multiple cracking observed in the plate at the ultimate bending moment region

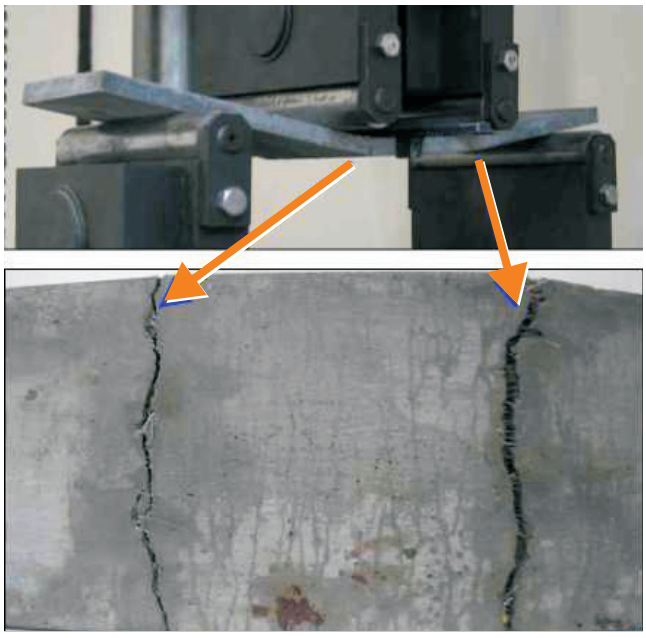

6.5 Direct tensile strength

A typical curve of stress behavior in tension versus elongation in UHPFRCC is shown in Figure 21.

A mean first crack stress is observed, indicated by point B, of 10.2 MPa (with 15.1% CV) corresponding to 0.026 mm elongation while the ultimate post-cracking stress (point C in Figure 21), of approximately 11.1 MPa (with 7.3% CV), corresponded to 0.213 mm elongation. Ultimate stress elongation is 8 times greater than the one observed in the first cracking. From point C, due to localization of a main crack, a strain-softening behavior could be observed. It is worth-mentioning that, even with such a high elongation as 0.4-0.5mm (15-20 times the first crack elongation), the UHPFRCC still withstood equivalent stresses to the one of first crack formation. Figure 22 shows the shape of rupture and the internal distribution of steel fibers in matrix at the region of rup-

Figure 21 – Typical stress curve in tension versus elongation

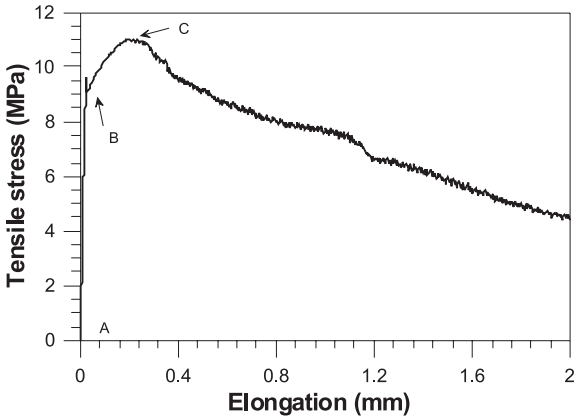

ture of elements tested. A homogeneous distribution can be seen along the cross-section.
The experimental results of tensile strength have overestimated the results forecast by the model at about 23%.

Figure 22 – Shape of rupture and internal distribution of fibers

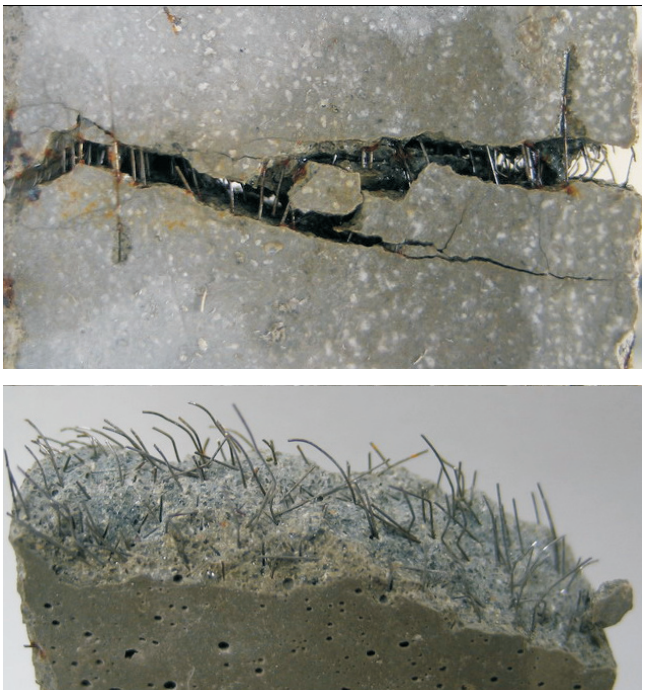

7 Conclusions

The present paper presented the mix design, production and mechanical characterization of a self-compacting ultra-high performance fiber reinforced cement composite, referred to as UHPFRCC.
A model developed within a theoretical and experimental scientific framework has been used for the mix design, which allows for compacity of a granular mix to be calculated. The model derived therefrom, called Compressive Packing Model (CPM) can be implemented in a computer code, allowing the optimization of the mixes. The CPM also allows for packing properties of the composite to be correlated in both the fresh and in the hardened states.
Thus, in view of outcomes presented, one can conclude that CPM has proven to be operational and accurate, having allowed for an ultra high performance material to be mixed.

8 Acknowledgements

The authors wish to acknowledge the invaluable collaboration of PETROBRAS, CAPES and CNPq for grants and scholarships provided for development of the present research.

9 Reference works

[01] Formagini, S., Dosagem Científica e Caracterização Mecânica de Concretos de Altíssimo Desempenho. Tese de Doutorado, COPPE/UFRJ, Rio de Janeiro, 2005, 284 p.
[02] Richard, P and Cheyrezy, M., Composition of Reactive Powder Concretes. Cement and Concrete Research, Vol. 25, N° 7, 1995, p. 1501-1511.
[03] Orange, G., Dugat, J. and Acker, P., Ductal: New Ultra High Performance Concretes. Damage Resistance and Micromechanical Analysis. Fifth RILEM Symposium on Fiber-Reinforced Concretes (FRC), Lyon, France, September 2000, p. 781-790.
[04] Formagini, S., Toledo-Filho, R. D., Fairbairn, E. M. R., Mix design and mechanical characterization of an ultra high performance fiber reinforced cement composites (UHPFRCC), in International Workshop on High Performance Fiber Reinforced Cementitious Composites in Structural Applications, Honolulu, USA, (RILEM, 2005).
[05] de Larrard, F., Formulation et Propriétés des Bétons à Très Hautes Performances. Thèse de Doctorat de l´Ecole Nationale des Ponts et Chaussées, Rapport de Recherche LPC N° 149, March 1988, Paris.
[06] de Larrard, F., Concrete Mixture Proportioning: a Scientific Approach, Modern Concrete Technology Series, E&FN SPON, London, 1999, 448 p.
[07] Sedran, T., Rhéologie et Rhéométrie des Bétons. Application aux Bétons Autonivelants. Doctoral Thesis of Ecole Nationale des Ponts et Chaussées, Paris, 1999, 220 p.

[08] Brandão, J. H., Projeto, Análise Experimental e Numérica de Cascas de Concretos de Ultra-Alto Desempenho Reforçado com Fibras. Tese de Doutorado, COPPE/UFRJ, Rio de Janeiro, 2005, 144 p.
[09] NBR NM 23, Cimento Portland e Outros Materiais em Pó - Determinação de Massa Específica. ABNT. Março, 2001.
[10] NBR 9776, Agregados – Determinação da Massa Específica de Agregados Miúdos por Meio do Frasco Chapman. ABNT, Março, 1987.
[11] Aïtcin, P. C., High-Performance Concrete. E&FN SPON, Thomas Telford, London, 1998, 591 p.
[12] Silva, A. S. M., Dosagem De Concreto Pelos Métodos De Empacotamento Compressível e Aïtcin-Faury Modificado. Dissertação de Mestrado, COPPE/UFRJ, Rio de Janeiro, 2004, 152 p.
[13] Tazawa, Ei-Ichi, Autogenous Shrinkage of Concrete. E & FN Spon, London, 1999, 424 p.
[14] Bazant, Zdenek P. and Planas, Jaime. Fracture and Size Effect in Concrete and Other Quasibrittle Materials. CRC Press, 1997, New York, 640 p.